The Astrophysical Journal, 837:30 (19pp), 2017 March 1 https://doi.org/10.3847/1538-4357/aa5c41


# An Update on Monitoring Stellar Orbits in the Galactic Center

S. Gillessen[1], P. M. Plewa[1], F. Eisenhauer[1], R. Sari[2], I. Waisberg[1], M. Habibi[1], O. Pfuhl[1], E. George[1], J. Dexter[1], S. von Fellenberg[1], T. Ott[1], and R. Genzel[1,3]
[1] Max-Planck-Institut für Extraterrestrische Physik, D-85748 Garching, Germany
[2] Racah Institute of physics, The Hebrew University, Jerusalem 91904, Israel
[3] Astronomy & Physics Departments, University of California, Berkeley, CA 94720, USA
*Received 2016 November 22; revised 2016 December 31; accepted 2017 January 17; published 2017 February 28*

## Abstract

Using 25 years of data from uninterrupted monitoring of stellar orbits in the Galactic Center, we present an update of the main results from this unique data set: a measurement of mass and distance to Sgr A*. Our progress is not only due to the eight-year increase in time base, but also to the improved definition of the coordinate system. The star S2 continues to yield the best constraints on the mass of and distance to Sgr A*; the statistical errors of $0.13 \times 10^6\,M_\odot$ and 0.12 kpc have halved compared to the previous study. The S2 orbit fit is robust and does not need any prior information. Using coordinate system priors, the star S1 also yields tight constraints on mass and distance. For a combined orbit fit, we use 17 stars, which yields our current best estimates for mass and distance: $M = 4.28 \pm 0.10|_{\rm stat.} \pm 0.21|_{\rm sys} \times 10^6\,M_\odot$ and $R_0 = 8.32 \pm 0.07|_{\rm stat.} \pm 0.14|_{\rm sys}$ kpc. These numbers are in agreement with the recent determination of $R_0$ from the statistical cluster parallax. The positions of the mass, of the near-infrared flares from Sgr A*, and of the radio source Sgr A* agree to within 1 mas. In total, we have determined orbits for 40 stars so far, a sample which consists of 32 stars with randomly oriented orbits and a thermal eccentricity distribution, plus eight stars that we can explicitly show are members of the clockwise disk of young stars, and which have lower-eccentricity orbits.

*Key words:* astrometry – black hole physics – Galaxy: center – Galaxy: fundamental parameters – techniques: high angular resolution

*Supporting material:* machine-readable tables

## 1. Introduction

The near-infrared regime is a sweet spot for studying the gravitational potential in the Galactic Center. To measure the latter, one would like to have as high a resolution as possible, and have access to the emission of objects compact and bright enough that they can serve as test particles for the potential. The optimum band is around 2 $\mu$m wavelength, where the extinction screen amounts to less than 3 mag (e.g., Nishiyama et al. 2009; Fritz et al. 2011), and where adaptive optics at 8 m class telescopes is performing well for typical atmospheric conditions. The intrinsic resolution of around 50 mas allows us to measure stellar orbits with semimajor axes of similar size, corresponding to orbital periods around a decade for a black hole of four million solar masses at 8 kpc distance.

Twenty-five years of near-infrared observations of the Galactic Center have shown that a wealth of fundamental astrophysical and physical questions can be addressed with these measurements, ranging from star formation, to stellar dynamics, to testing general relativity (Genzel et al. 2010). The outstanding, main result of these observations is that they provide direct and tight constraints on the nature of Sgr A*: This is the massive black hole (MBH) at the center of the Milky Way. The key to this result is that one can measure the mass of Sgr A* by tracing individual stellar orbits around it. If a sufficiently large part of an orbit is sampled, one can deduce information on the potential through which the star is moving. In particular, one can determine the central mass and the distance to it. Due to its proximity, the Galactic Center is the only galactic nucleus where such an experiment is currently feasible.

A geometric determination of the distance to the Galactic Center, $R_0$, is important for many branches of astronomy. $R_0$ is one of the fundamental parameters of any model of the Milky Way, and its value determines mass and size of the Galaxy. This ties $R_0$ into the cosmological distance ladder, since galactic variables serve as zero point for the period–luminosity relations determined usually in the Large Magellanic Cloud. The mass of the MBH is equally important. Using this value, one can place the Milky Way onto scaling relations (Kormendy & Ho 2013). Knowing the mass of and distance to Sgr A* is the reason why the Galactic Center is a unique testbed concerning MBHs and their vicinities for numerous models in many branches of astrophysics (Yuan & Narayan 2014). The Milky Way also serves as a check for mass measurements in other galaxies, since the true black hole mass is known and one can simulate observations at lower resolution (Feldmeier et al. 2014).

The most profound result of the orbital work is the proof of existence of astrophysical MBHs. This opens up a new route for testing general relativity, at a mass scale and a field curvature that have not been accessible so far. Since the fundamental parameters are known for Sgr A*, one can think of more ambitious experiments using the black hole. Most notably, in the near future two observations might become feasible. (i) Using the motions of stars and/or that of plasma radiating very close to the event horizon, one might be able to measure the spin of the black hole. The instrumental route to that goal is near-infrared interferometry (Eisenhauer et al. 2011). (ii) A global radio-interferometric array operating at around 1 mm should be able to resolve Sgr A*, i.e., to deliver an actual image of the black hole's shadow (Luminet 1979; Falcke et al. 2000; Doeleman et al. 2008). Additionally, the

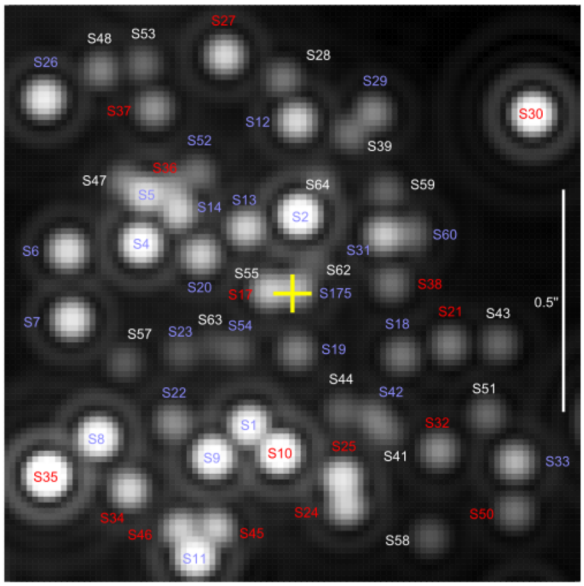


**Figure 1.** Mock image of the central arcsecond for our reference epoch 2009.0, constructed from the measured motions and magnitudes of the stars, assuming a point-spread function size and pixel sampling as in our NACO data. Stars with spectral identification have colored labels: blue for early-type stars (Br-$\gamma$ absorption line detected) and red for late-type stars (CO band heads detected). The yellow cross denotes the position of Sgr A*. For a wider view see Figure 15.

most stringent tests of general relativity would be possible if a pulsar representing a perfect clock in a short-period orbit around Sgr A* were found (Psaltis et al. 2016).

Here, we report on updates to our ongoing, long-term program of monitoring stellar orbits around Sgr A*. The first orbit determination dates back to 2002 (Schödel et al. 2002; Ghez et al. 2003). A few years later, orbits for a handful of stars had been determined (Eisenhauer et al. 2005; Ghez et al. 2005), and after a few more years, the number of known orbits exceeded 20 (Gillessen et al. 2009b). The number of known orbits has now risen to around 40, and both statistical and systematic errors of our measurements are much reduced compared to previous measurements.

## 2. Data

This work is an update and improvement over our previous orbital study (Gillessen et al. 2009b). The two main improvements are stated here.

1. Since the previous work we have added eight more years of data, using the adaptive optics (AO) imager NACO on the VLT (Lenzen et al. 1998; Rousset et al. 1998) and the AO-assisted integral field spectrograph SINFONI (Bonnet 2003; Eisenhauer et al. 2003). This extends our time base from 17 to 25 years for the imaging and from five to 13 years for the spectroscopy. We add (in the best cases) 78 epochs of imaging and 19 epochs of spectroscopy.
2. We implement the improved reference frame described in Plewa et al. (2015). This greatly improves our prior knowledge, where we expect an orbit fit to reconstruct the mass responsible for the orbital motion of the S-stars. The new calibration links to the International Celestial Reference Frame (ICRF) in a two-step procedure, and compared to our previous work does not rely on the assumption that the mean motion of a large sample of stars observed around Sgr A* is zero.

The other steps of the analysis are identical, and we refer the reader to Gillessen et al. (2009b) for more details. In particular, the following critical issues are treated as before.

1. The assignment of statistical errors to individual data points.
2. The relative weight between the earlier Speckle data (1992–2001, Hofmann et al. 1992) and the AO data is unchanged. We weigh down the NACO-based astrometric data by a global factor 1.42, determined in Gillessen et al. (2009b) as the factor which makes the noise in the AO data match the statistical error estimates.
3. The errors assigned to S2 in 2002 are identical to those derived in the previous work. S2 may have been confused and its position perturbed in 2002, when the star passed the pericenter of its orbit.

Our imaging data set contains an interruption. During 2014 and in spring 2015, NACO was not available at the VLT, resulting in significant gaps in our time series. In summer 2015 NACO resumed operation (now at UT1, no longer at UT4). The data obtained after that (ten epochs) show that we can reconstruct the stellar positions to the same level of precision as before. Also, there is no systematic mismatch between the positions obtained before and after. We therefore do not need to apply any corrections related to the interruption.

For orbits fits using a combined data set of both VLT- and Keck-based observations, we replace the data points of Ghez et al. (2008) by the newer publication from the same team of Boehle et al. (2016). Figure 1 gives an overview of the crowded stellar field in the central arcsecond.

## 3. The Gravitational Potential in the Galactic Center

### 3.1. Orbit Fitting

Orbit fitting has a relatively large number of free parameters. While in its most simple form the potential has only one free physical parameter (the central mass $M$), we do not know a priori where the mass is located and how it moves. Hence six additional parameters need to be determined simultaneously: the distance to the mass $R_0$, its position on the sky ($\alpha$, $\delta$) and its motion ($v_\alpha$, $v_\delta$, $v_z$). Acceleration terms are not needed at the current level of precision (Reid & Brunthaler 2004). Furthermore, the orbit of the star that is probing the potential needs to be determined at the same time. The orbit parameters are essentially the initial conditions for its motion in the potential (three position variables and three velocity variables), which conventionally are expressed in terms of the classical orbital elements ($a$, $e$, $i$, $\Omega$, $\omega$, $t_P$).[4] Therefore the most simple orbit fit has already 13 free parameters. For $n$ stars, one has $7 + 6 \times n$ free parameters.

For the six coordinate system parameters of the potential we have prior knowledge. $R_0$ has been determined in multiple ways; for a recent review see Bland-Hawthorn & Gerhard (2016), who conclude $R_0 = 8.2 \pm 0.1$ kpc from averaging the

[4] Here, $a$ is the semimajor axis of the orbit, $e$ the eccentricity, $i$ the inclination, $\Omega$ the position angle of the ascending node, $\omega$ the longitude of the pericenter, and $t_P$ the epoch of pericenter passage.

results of many individual determinations. As $R_0$ is one of the parameters we wish to determine, we do not use the prior information for it.

Since we correct our radial velocity measurements to the local standard of rest (LSR), and the expected motion of Sgr A* is very small (below 1 km s$^{-1}$, Reid & Brunthaler 2004) we expect $v_z = 0$, with an uncertainty due to the uncertainty of the LSR of around 5 km s$^{-1}$. For the position on the sky and the motion in the plane of the sky of Sgr A*, we can adopt the limits from Plewa et al. (2015): $(\alpha, \delta) = (0, 0) \pm (0.2, 0.2)$ mas at our reference epoch 2009.0, and $(v_\alpha, v_\delta) = (0, 0) \pm (0.1, 0.1)$ mas yr$^{-1}$. These priors only show very small covariances, which we neglect in our analysis.

We use a fitting code we developed in Mathematica (Wolfram Research, Inc. 2016), which calculates the positions and velocities by explicitly integrating the orbits, and then uses the built-in minimization routines to find the best fitting parameters. These routines are based on standard techniques such as quasi-Newton methods, steepest gradient search, or the Levenberg–Marquardt algorithm. Usually, we apply different search algorithms iteratively, until none is able to improve the minimum further. Our code also allows the use of (or omission of) prior information for the parameters to be solved for. We can either obtain the parameter errors from the inverse of the correlation matrix or from the parameter distributions as output by a Markov chain. Our fitting routine also allows fitting for more complicated orbit models, and in particular we can include relativistic corrections. We have implemented the potential of the Schwarzschild metric (Will 2008), the gravitational redshift, the transverse Doppler effect, and the Roemer time delay (Zucker et al. 2006). Also, it is possible to integrate the orbits in the potential of an extended mass distribution.

We explicitly tested our implementation of the Schwarzschild precession term. We fitted a simulated, relativistic orbit of the star S2 (i.e., in the weak-field limit) for a full orbital period (from $t = 0$ to $t = T$), which yielded back the parameters put into the simulation. Simulating the same orbit from $t = T$ to $t = 2T$ and fitting it yielded back these parameters again, except for $\omega$ (the longitude of periastron describing the orientation of the ellipse in its plane), which had changed by the amount expected from the formula

$$\Delta\omega = 6\pi \frac{G\,M}{c^2} \frac{1}{a\,(1 - e^2)}. \quad (1)$$

### 3.2. The Potential Based on S2 Only

Most of our knowledge of the MBH's potential is due to a single star, S2, which happens to be comparably bright ($m_K \approx 14$) and orbits Sgr A* on a short-period orbit ($P = 16$ years). It is the brightest star for which we can determine an orbit and hence is less prone to errors due to confusion than all other stars. Its orbital period of around 16 years is the second shortest known. We investigate the potential we can derive from S2 alone before including data from more stars.

We first fit the orbit of S2 without using any coordinate system prior information (row 1 in Table 1). The 2D coordinate system parameters from the fit are consistent with what we expect from the priors, and we can repeat the fit using the priors as additional constraints (row 2). We also repeat the fit from Gillessen et al. (2009a) in row 3, which includes into our data set the publicly available S2 data from Boehle et al. (2016). This comes at the cost of having to solve for four additional parameters, namely the difference between the two reference frames. One can see from the parameter errors that the additional information by including the Keck data is countered by the inclusion of the four additional free parameters. The combination of the two data sets therefore does not constrain the potential further in a substantial way, although one might have expected that the Keck data would help for the years 1995–2001, where our data set is based on lower Strehl ratio Speckle-imaging at the smaller 3.6 m ESO NTT on La Silla. Figure 2 shows the positional and velocity data and the best-fitting orbit, for the case where the priors and the Keck data have been used in addition to our raw data set. We refer to it as the "combined" fit. It constitutes our best estimate for the S2 orbit and the corresponding potential:

$$M = 4.35 \pm 0.13 \times 10^6\,M_\odot$$
$$R_0 = 8.33 \pm 0.12\ \mathrm{kpc}.$$

These errors are only the formal fit errors, the additional systematic errors for S2 are determined in Section 3.2.3. As a cross check, we also fit the combined S2 data set without using any priors (row 4 in Table 1). Again, the resulting parameters do not deviate significantly between a fit using the priors (row 3) or not (row 4). We conclude that the inclusion of the Keck data does not introduce any significant systematic errors related to the difference in coordinate systems.

After using a classical minimization routine, we also run a Markov chain Monte Carlo (MCMC) routine, which we started at the previously determined best-fit position and which we ran for at least $2 \times 10^5$ steps. Since the posterior distribution is compact, this approach is sufficient. As expected, the chain never hit any point in parameter space with a smaller $\chi^2$. The posterior distribution has more information about the parameter uncertainties. Table 1 also gives the associated errors. The parameter uncertainties obtained from the formal error matrix and from the MCMC agree. In Figure 3 we show the marginal posterior distribution of $R_0$ and $M_{\mathrm{MBH}}$ for the fits given in rows 1–3 of Table 1. A more complete view of the chain output is given in the Appendix in Figure 14, where we show the two-dimensional projections for the 13 parameters (excluding the four needed to describe the coordinate system mismatch between our data and the Keck data). The figure shows explicitly that the posterior distribution is compact, and that all parameters are well-constrained.

The mass of and distance to Sgr A* are highly correlated parameters. Using the S2 data, for a given distance, the corresponding mass is

$$M\,(R) = (4.005 \pm 0.033) \times 10^6 M_\odot \times (R_0/8\ \mathrm{kpc})^{2.00}. \quad (2)$$

The mass uncertainty for a given distance is below 1%.

The fit of the MPE-only data set without priors in row 1 of Table 1 yields a somewhat large radial velocity of the central mass of 28 km s$^{-1}$. This might be connected to a systematic error of measuring radial velocities, see Section 3.2.3. In order to decouple the fit from such a bias, but still being able to profit from the 2D priors, we have repeated the fit with 2D priors only. This fit yields again a systemic radial velocity of around 25 km s$^{-1}$. The distance estimate is $R_0 = 8.35$ kpc then, very close to what our fiducial fit yields (row 3).

We also tested whether allowing for a constant rotation speed of the coordinate system would make a difference in the fits.

**Table 1**
The Gravitational Potential Based on Orbital Fitting

| # | Data | Priors | Type | $R_0$ (kpc) | $M_{\rm MBH}$ ($10^6 M_\odot$) | $\alpha$ (mas) | $\delta$ (mas) | $v_\alpha$ ($\mu$as yr$^{-1}$) | $v_\delta$ ($\mu$as yr$^{-1}$) | $v_z$ (km s$^{-1}$) | r. $\chi^2$ |
|---|---|---|---|---|---|---|---|---|---|---|---|
| 1 | S2, VLT | none | Kepl. | $8.17 \pm 0.20$ | $4.25 \pm 0.20$ | $0.23 \pm 0.39$ | $-2.10 \pm 0.61$ | $88 \pm 40$ | $-2 \pm 63$ | $28.3 \pm 7.0$ | 1.19 |
| | MCMC errors | | | $^{+0.17}_{-0.23}$ | $^{+0.18}_{-0.22}$ | $^{+0.39}_{-0.40}$ | $^{+0.53}_{-0.69}$ | $^{+41}_{-40}$ | $^{+67}_{-61}$ | $^{+6.4}_{-8.2}$ | |
| 2 | S2, VLT | 2D, $v_z$ | Kepl. | $8.13 \pm 0.15$ | $4.10 \pm 0.16$ | $-0.31 \pm 0.34$ | $-1.29 \pm 0.44$ | $78 \pm 37$ | $126 \pm 47$ | $8.9 \pm 4.0$ | 1.28 |
| | MCMC errors | | | $^{+0.13}_{-0.16}$ | $^{+0.14}_{-0.16}$ | $^{+0.34}_{-0.34}$ | $^{+0.43}_{-0.45}$ | $^{+37}_{-37}$ | $^{+47}_{-46}$ | $^{+3.9}_{-4.0}$ | |
| 3 | S2, comb. | 2D, $v_z$ | Kepl. | $8.33 \pm 0.12$ | $4.35 \pm 0.13$ | $0.96 \pm 0.21$ | $-1.28 \pm 0.32$ | $-45 \pm 23$ | $120 \pm 33$ | $5.0 \pm 3.6$ | 1.48 |
| | MCMC errors | | | $^{+0.12}_{-0.12}$ | $^{+0.13}_{-0.14}$ | $^{+0.21}_{-0.21}$ | $^{+0.32}_{-0.34}$ | $^{+34}_{-33}$ | $^{+23}_{-23}$ | $^{+3.5}_{-3.7}$ | |
| | $\Delta$ sys. | | | | | $-0.81 \pm 0.21$ | $-0.83 \pm 0.21$ | $-85 \pm 20$ | $462 \pm 21$ | | |
| | MCMC errors | | | | | $^{+0.22}_{-0.20}$ | $^{+0.22}_{-0.22}$ | $^{+19}_{-21}$ | $^{+21}_{-22}$ | | |
| 4 | S2, comb. | none | Kepl. | $8.17 \pm 0.15$ | $4.30 \pm 0.15$ | $1.49 \pm 0.24$ | $-2.41 \pm 0.49$ | $-34 \pm 24$ | $24 \pm 44$ | $11.5 \pm 5.4$ | 1.41 |
| | MCMC errors | | | $^{+0.15}_{-0.15}$ | $^{+0.16}_{-0.15}$ | $^{+0.23}_{-0.25}$ | $^{+0.49}_{-0.49}$ | $^{+25}_{-24}$ | $^{+44}_{-45}$ | $^{+5.5}_{-5.5}$ | |
| | $\Delta$ sys. | | | | | $-0.50 \pm 0.22$ | $-1.06 \pm 0.23$ | $-114 \pm 21$ | $485 \pm 22$ | | |
| | MCMC errors | | | | | $^{+0.20}_{-0.23}$ | $^{+0.23}_{-0.23}$ | $^{+22}_{-20}$ | $^{+22}_{-22}$ | | |
| 5 | S1 | 2D, $v_z$ | Kepl. | $8.47 \pm 0.18$ | $4.45 \pm 0.28$ | $-0.89 \pm 1.27$ | $-0.19 \pm 1.31$ | $80 \pm 139$ | $17 \pm 143$ | $-0.1 \pm 7.4$ | 2.21 |
| 6 | S9 | 2D, $v_z$ | Kepl. | $8.08 \pm 0.78$ | $4.04 \pm 1.26$ | $0.21 \pm 1.51$ | $0.10 \pm 1.52$ | $-38 \pm 164$ | $-17 \pm 165$ | $0.0 \pm 8.3$ | 2.73 |
| 7 | S13 | 2D, $v_z$ | Kepl. | $8.74 \pm 0.97$ | $4.84 \pm 1.59$ | $-0.22 \pm 2.60$ | $2.22 \pm 2.57$ | $86 \pm 291$ | $-296 \pm 277$ | $-3.1 \pm 15.5$ | 10.6 |
| 8 | S2, comb. | 2D, $v_z$ | GR | $8.41 \pm 0.13$ | $4.43 \pm 0.14$ | $0.58 \pm 0.21$ | $-1.31 \pm 0.33$ | $-16 \pm 23$ | $120 \pm 34$ | $1.5 \pm 3.6$ | 1.47 |
| 9 | **Multi** | **2D,** [illegible] | **Kepl.** | $8.32 \pm 0.07$ | [illegible] $\pm$ [illegible] | $-0.08 \pm 0.37$ | $-0.89 \pm 0.31$ | $39 \pm 41$ | $58 \pm 37$ | $14.2 \pm 3.6$ | **0.98** |
| 10 | w/o S2 | 2D, $v_z$ | Kepl. | $8.19^{+0.16}_{-0.11}$ | $4.08^{+0.25}_{-0.14}$ | $0.55^{+0.65}_{-0.62}$ | $-0.26^{+0.64}_{-0.60}$ | $-83^{+0.69}_{-0.73}$ | $-22^{+0.65}_{-0.70}$ | $7.0^{3.7}_{-3.6}$ | 0.97 |

**Note.** The first four fits use the S2 data and differ in whether or not the Keck data are used, and whether or not we include coordinate system priors in the fit. For each fit we report the best-fitting parameters and the associated uncertainties as obtained by the error matrix. For S2, we also report the uncertainties as obtained by running a Markov chain Monte Carlo routine. The $1\sigma$ error intervals are constructed as symmetric confidence intervals around the best-fitting value. Rows 5 to 7 give the same parameters as obtained from fitting S1, S9, and S13 individually. For these stars, the errors have been scaled up by the square root of the reduced $\chi^2$ (last column), corresponding to a rescaling such that reduced $\chi^2 = 1$. Row 8 presents a relativistic fit for the combined S2 data. Row 9 (bold) gives the multi-star fit using 17 stars simultaneously. The errors are taken from the Markov chain, and the reduced $\chi^2$ is smaller than 1 since before starting the fit all stars have been individually rescaled such that their respective reduced $\chi^2 = 1$. This is our best fit overall. Row 10 is the result of the multi-star fit excluding S2.

Using the combined S2 data set, the parameter corresponding to rotation has its best-fit value at $(-0.006 \pm 0.017)^\circ$ yr$^{-1}$, not significantly deviating from zero. The distance estimate is basically unchanged: $R_0 = 8.34$ kpc. We conclude that we can neglect rotation. Furthermore, from the definition of the coordinate system we can set a prior on its rotation of $0^\circ.00004$ yr$^{-1}$ (Plewa et al. 2015), which is essentially the same as fixing it at zero. For simplicity we do the latter.

#### 3.2.1. Relativistic Fit

Using a general relativistic orbit model, the S2 based mass and distance are

$$M = 4.43 \pm 0.14 \times 10^6\, M_\odot$$
$$R_0 = 8.41 \pm 0.13 \text{ kpc}.$$

We note that the values increase moderately compared to the respective Keplerian fits. It was already noted by Zucker et al. (2006) that the Keplerian fit yields biased parameter estimates for a relativistic orbit, although the size (and sign) of these biases has not yet been studied systematically.

In the orbit fitting tool, we can check the effect of the four relativistic corrections implemented independently. After rescaling the error bars such that the Keplerian (combined) S2 fit yields a reduced $\chi^2$ of 1, we tested models with the different effects, or combination of those, one by one. This yielded reduced $\chi^2$ values between $\approx$0.987 and $\approx$1.020. For the 414 degrees of freedom a $1\sigma$-significant deviation would be reached for $\Delta\chi^2_{\rm red} = \sqrt{2/\rm dof} = 0.070$ (Andrae et al. 2010). Hence, we cannot distinguish between any of these models, and cannot detect any of the leading-order relativistic effects: Schwarzschild precession, gravitational redshift, relativistic Doppler effect, and Roemer delay. The Keplerian description continues to suffice.

#### 3.2.2. Limits on an Extended Mass Component

Fitting the combined S2 data using an additional, extended mass component with a Plummer profile

$$\rho(r) = \frac{3}{8\pi} M_{\rm ext}\, r_s^{-3} \left[\frac{r}{r_s}\right]^{-5/2} \quad (3)$$

with a scale radius of $r_s = 0''.4$ yields that $-0.4 \pm 1.2\%$ of the mass of the MBH is in the extended component, where we have allowed $M_{\rm ext}$ to also take negative values. This corresponds to $-0.3 \pm 0.7\%$ between pericenter and apocenter of the S2 orbit, the radial range where our data are sensitive to an additional mass component. Changing $r_s$ to $0''.125$ yields a very similar result, with $-0.5 \pm 0.8\%$ being in the extended component or $-0.3 \pm 0.5\%$ inside the S2 orbit. We also used a power-law density profile with $\rho(r) \propto r^{-7/4}$, making the extended mass component inside the S2 orbit $-0.5 \pm 0.8\%$.

We conclude that our data are consistent with a pure point mass, and can place a conservative upper limit on a possible extended component inside the S2 orbit at 1% of the mass of the MBH.

#### 3.2.3. Systematic Errors for S2

A main source of uncertainty in Gillessen et al. (2009b) was the weight of the S2 data in 2002. A fit using S2 only leaving

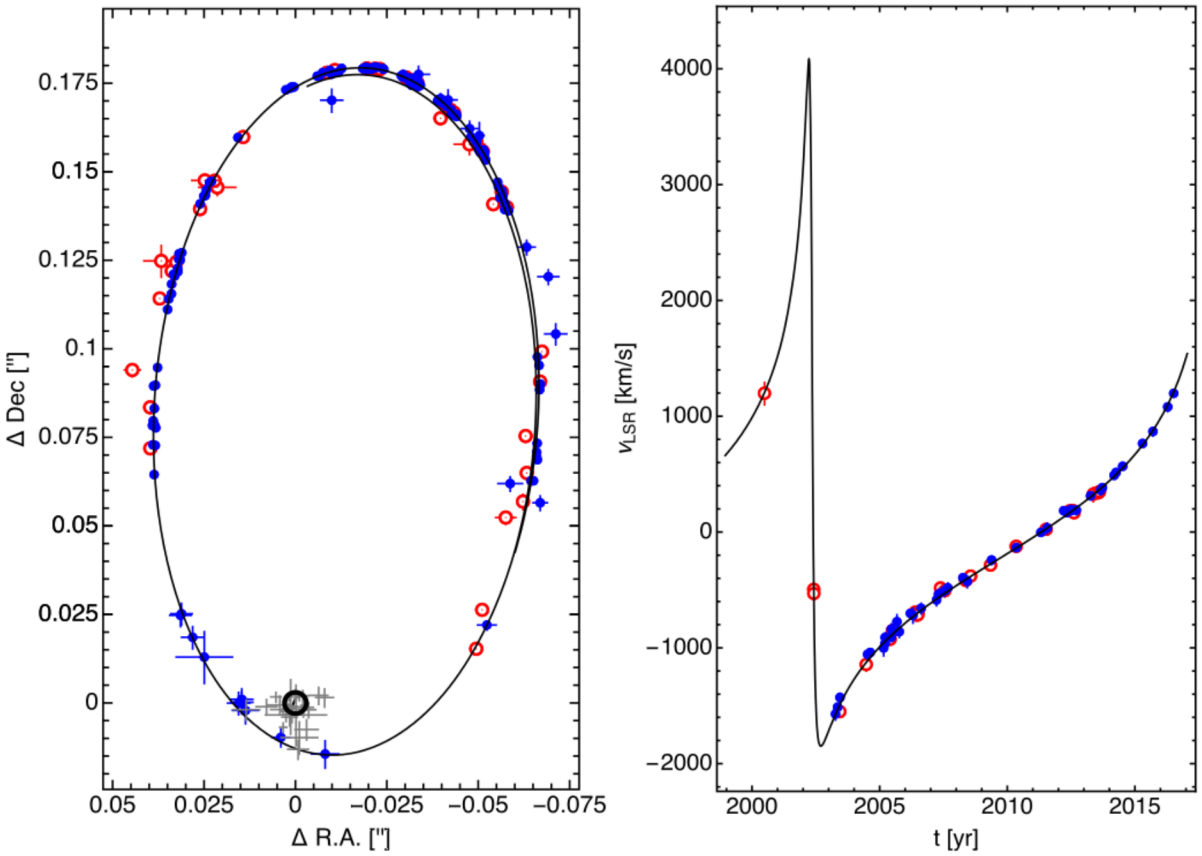


**Figure 2.** Orbit of the star S2. Left: the measured positions plotted in the plane of the sky. The blue data are from the VLT (before 2002: from the NTT), and the red data are from Boehle et al. (2016) corrected for the difference in reference coordinate system. The gray data points are positions at which flares have been recorded. The black ellipse is the best-fitting orbit, and the position of the mass is denoted by the black circle. Note that the fitting procedure matches the functions $\alpha(t)$ and $\delta(t)$, i.e., it does not only match the positions in the plane of the sky but rather also in time. The plotted ellipse does not close, since there is a small residual drift motion of the fitted mass in the reference frame. The physical model is purely Keplerian. Right: the measured radial velocities as a function of time. The same best-fitting orbit as in the left panel is denoted by the black line.

out the 2002 data yielded a distance value as low as $R_0 = 7.4$ kpc, while using the 2002 data with their full weights yielded $R_0 = 8.9$ kpc. The corresponding range of values of $R_0$ for the updated (combined VLT and Keck) data set now is $8.24\,\mathrm{kpc} < R_0 < 8.84\,\mathrm{kpc}$, i.e., it has reduced by more than a factor of 2.

The influence of individual data points on the fit result can be checked by bootstrapping. For that we created 1000 bootstrapped files by drawing randomly with replacement of as many data points from a given star's data as there are measurements. Some data points are thus repeated in the bootstrapped file; others are omitted. These mock data sets are then fit in the standard way, and the distribution of best-fitting parameters is a measure for the uncertainty in the data. Figure 4 shows in the leftmost panel the results for the (VLT-only) S2 data set. The associated error bars are $\pm 0.13$ kpc for $R_0$ and $\pm 0.13 \times 10^6\,M_\odot$ for $M$, i.e., comparable to the statistical fit uncertainties. The second panel in Figure 4 shows the combined uncertainties from bootstrapping and the Markov chain. For that figure we assumed that the statistical fit errors at the best-fit position are valid at each point of the bootstrap.

While we expect instrumental systematics in $v_{LSR}$ to average out, the shape of the stellar absorption lines for the massive B dwarfs might be affected by stellar winds. This results in a systematic difference of measured radial velocity and true radial velocity of the center of mass of the star. We estimate that such effects could bias the measurements at the 20 km s$^{-1}$ level. For S2, a star for which we have measured positive and negative radial velocities, this would be absorbed into the radial motion of the coordinate system $v_z$, and indeed, the S2 fits without prior information (rows 1 and 4 in Table 1) yield a value of $v_z$ of roughly that amount.

By including the difference between the S2 fits with or without coordinate system prior information we cover not only the coordinate system uncertainty, but also the possible biases due to the line shape of the absorption lines. We use the mean of the half difference between the fits in rows 1 and 2, and rows 3 and 4 as contributions to the systematic error: This adds 0.05 kpc to the error budget.

The difference in $R_0$ between the Keplerian and the relativistic model amounts to 0.09 kpc for S2. Since we have not explicitly detected relativistic effects, we include half of this in the systematic error. Similarly, we account for the models using an extended mass component, adding 0.01 kpc only.

Adding the contributions in squares, we estimate the systematic error of the S2-based distance estimate to be 0.17 kpc.

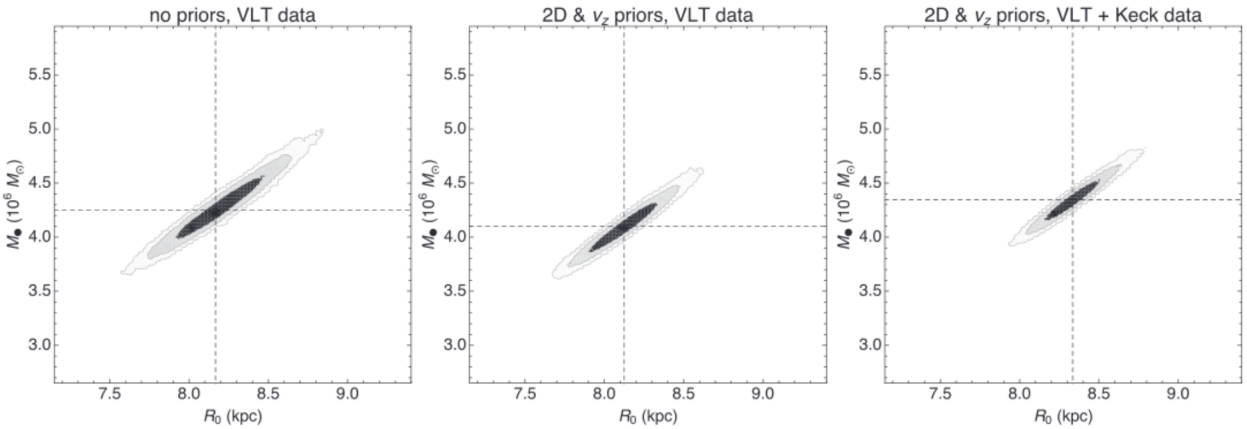


**Figure 3.** Mass of and distance to Sgr A* from the orbit of S2. The three panels show projections of the respective Markov chains into the mass–distance plane, giving contours at the 1, 2, and 3$\sigma$ level. The dashed lines mark the best-fit values. The left panel is for a fit without prior information (row 1 in Table 1); the middle panel includes the priors and thus leads to smaller parameter uncertainties (row 2 in Table 1). The right panel in addition uses the Keck data from Ghez et al. (2008), which leads to a small shift of the best-fitting parameters with virtually unchanged uncertainties (row 3 in Table 1).

### 3.3. The Potential Based on S1

S1 is the second-best star in terms of how much it constrains Sgr A*'s potential (Figure 5). We can follow the trajectory of this $m_K = 14.8$ star over the full time range from 1992 to 2016, and it does not suffer from any apparent confusion. It passed the pericenter of its orbit in mid-2001. If one applies the coordinate system priors, S1 yields a similarly good constraint on $R_0$ as S2. The best-fit parameters and statistical errors for S1 are (row 5 in Table 1):

$$M = 4.45 \pm 0.28 \times 10^6\, M_\odot$$
$$R_0 = 8.47 \pm 0.18 \text{ kpc}. \quad (4)$$

Without the priors, the S1 fit is not well constrained, and no useful constraints on $M$ and $R_0$ can be obtained. This is in contrast to the fit of S2, for which the prior information is not essential. We have three possible ways to include prior information for S1. First, we can apply the coordinate system priors as obtained from Plewa et al. (2015). This assumes that the radio source Sgr A* is the counterpart to the mass. This method of including the coordinate system prior results in the numbers given in Equation (4) and row 5 in Table 1. The second option is to use the results from the S2 fit without priors as coordinate system priors for S1. This assumes that the two stars orbit the same mass. This fit yields $M = 4.55 \pm 0.29 \times 10^6\, M_\odot$ and $R_0 = 8.58 \pm 0.19$ kpc. The third option again assumes that S1 and S2 orbit the same mass: a simultaneous fit of the two data sets yields $M = 4.69 \pm 0.14 \times 10^6\, M_\odot$ and $R_0 = 8.63 \pm 0.10$ kpc. The agreement at the 1$\sigma$ level between these numbers shows that the method by which the prior information is included does not matter.

Another difference between S1 and S2 is that the error ellipse of S1 is oriented more steeply, $M \propto R_0^3$. For the following discussion it is useful to introduce

$$\mu := \frac{M}{R_0^3} = \frac{4\pi^2}{G}\frac{\alpha^3}{T^2}, \quad (5)$$

where $G$ is the gravitational constant, $\alpha$ the angular size of the semimajor axis, and $T$ the orbital period. For a data set with astrometry points only, one cannot measure mass and distance separately; instead one has a complete degeneracy $M \sim R_0^3$ or, in other words, one constrains $\mu$. When measuring $\mu$, the only quantities that enter are the angular size of the semimajor axis and the orbital period, which both can be determined from astrometry only. For a star with both astrometry and spectroscopy, $M \sim R_0^\alpha$ with $\alpha \gtrsim 3$, for example $\alpha = 2.00$ for our S2 data set. In the case that one has only a single radial velocity and an astrometric orbit, the error ellipsoid is oriented along the $R_0$- and $\mu$-axes, and its extension in the $R_0$-direction is given by the accuracy of the radial velocity point and by how much the inclination is degenerate with $R_0$. The latter degeneracy is severe for an (almost) face-on orbit with $i \approx 0$: If one changes $R_0$ by a factor $f$, one can find a good orbit fit at $M' = f^3 M$ and $i' = i/f^2$.

The error ellipses in the $M$–$R_0$-plane for S1 are surprising in two aspects, given that the orbital phase coverage is less than $\pi$ for S1, while the coverage is more than a full revolution for S2. First, the S1 data yield as good a constraint on $R_0$ as do those of S2 and, second, the S1 error ellipses are thinner than those from S2.

The first surprise can be explained in the following way. For S1, the radial velocity did not change much over the period covered by the measurements. The data can therefore be approximated by having, in addition to the astrometry, essentially a single, but very well measured radial velocity (with an uncertainty of around $\sigma_v/\sqrt{N_{\rm data}} \approx 15\,\mathrm{km\,s^{-1}}$). One has thus an error ellipsoid along the $\mu$-axis. Having a single radial velocity data point with a relative error of around $(15\,\mathrm{km\,s^{-1}})/(1100\,\mathrm{km\,s^{-1}}) = 1.4\%$ yields a distance error in the percent regime, up to a geometry factor depending of the shape and orientation of the orbit, which is not a large factor for S1's orbit. The distance estimate comes from the comparison of the radial velocity (in $\mathrm{km\,s^{-1}}$) with the proper motion (in $\mathrm{mas\,yr^{-1}}$). Compared with S2, the mean (absolute) radial velocity for S1 is actually higher, such that it is plausible that S1 can yield a similarly tight constraint on $R_0$.

The second surprise is that S1 yields a very good constraint on $\mu$, the ellipse is even tighter in the $\mu$-direction as is the S2 ellipse in the $M/R_0^2$ direction. To eliminate the influence of the